CHEMICAL PHYSICS LETTERS

Editors: ***D.C. Clary*** *(University of Oxford, Oxford, UK) and* ***M. Okumura*** *(California Institute of Technology, Pasadena, California, USA)*

ISSN: 0009-2614; IMPACT FACTOR: 1.860

Accepted August 19th 2016

A NUMERICAL STUDY OF MAGNETOHYDRODYNAMIC TRANSPORT OF NANOFLUIDS FROM A VERTICAL STRETCHING SHEET WITH EXPONENTIAL TEMPERATURE-DEPENDENT VISCOSITY AND BUOYANCY EFFECTS

Noreen Sher Akbar*
DBS&H CEME, National University of Sciences and Technology, Islamabad, ***Pakistan.***
Dharmendra Tripathi
Department of Mechanical Engineering, Manipal University, Jaipur-303007, ***India****.*
Zafar Hayat Khan
Department of Mathematics, University of Malakand, Dir (Lower), Khyber Pakhtunkhwa, ***Pakistan****.*
O. Anwar Bég
Fluid Mechanics, Aeronautical and Mechanical Engineering, School of Computing, Science and Engineering, University of Salford, Manchester, M54WT, ***UK***

**Corresponding Author: Email: noreensher@yahoo.com*

ABSTRACT

In this paper, a mathematical study is conducted of steady incompressible flow of a temperature-dependent viscous nanofluid from a vertical stretching sheet under applied external magnetic field and gravitational body force effects. The Reynolds exponential viscosity model is deployed. Electrically-conducting nanofluids are considered which comprise a suspension of uniform dimension nanoparticles suspended in viscous base fluid. The nanofluid sheet is extended with a linear velocity in the axial direction. The Buonjiornio model is utilized which features Brownian motion and thermophoresis effects. The partial differential equations for mass, momentum, energy and species (nano-particle concentration) are formulated with magnetic body force term. Viscous and Joule dissipation effects are neglected. The emerging nonlinear, coupled, boundary value problem is solved numerically using the Runge–Kutta fourth order method along with a shooting technique. Graphical solutions for velocity, temperature, concentration field, skin friction and Nusselt number are presented. Furthermore stream function plots are also included. Validation with Nakamura's finite difference algorithm is included. Increasing nanofluid viscosity is observed to enhance temperatures and concentrations but to reduce velocity magnitudes. Nusselt number is enhanced with both thermal and species Grashof numbers whereas it is reduced with increasing thermophoresis parameter and Schmidt number. The model is applicable in nano-material manufacturing processes involving extruding sheets.

KEY WORDS: *MHD flow; Variable viscosity nanofluids; Hartmann number; Reynolds number; Buoyancy; Stretching sheet; Schmidt number; Nusselt number; numerical.*

NOMENCLATURE

B_C Local solutal Grashof number
B_0 Magnitude of magnetic field strength
C Nano-particle (solutal) concentration
C_∞ Ambient nano-particle concentration in free stream
C_w Nano-particle (solute) concentration at the wall
C_w Nano-particle (solute) concentration at the wall
D_B Brownian diffusion coefficient
D_T Thermophoretic diffusion coefficient
g Acceleration due to gravity
G_T Local thermal Grashof number
K Thermal conductivity of the fluid
Le Regular Lewis number
M Hartmann Number
N_b Brownian motion parameter
Nt Thermophoresis parameters
Nu_x Local Nusselt number
P Pressure
P_r Prandtl number
q Heat flux
Sc Schmidt number (= *Pr Le*)
Sh_x^n Local nanoparticle Sherwood number
T Local fluid temperature
T_∞ Ambient temperature
u, v Velocity components along x and y directions
x, y Coordinate along and normal to the sheet

Greek Letters

α Reynolds viscosity parameter
η Similarity variable (transformed coordinate)
ϕ Nanoparticle volume fraction
θ Dimensionless temperature
$(\rho c)_f$ Heat capacity of the base fluid
$(\rho c)_p$ Effective heat capacity of the nanoparticle material
μ Dynamic viscosity of nanofluid
ν Kinematic viscosity of nanofluid

1. INTRODUCTION

Currently there is significant activity in applied physics and engineering sciences focused on elaborating and optimizing the performance characteristics of nanomaterials. These studies are driven by the need to fulfil the demands for high-efficiency performance and compact design of devices in numerous sectors including aerospace, mechanical, chemical, energy systems and biomedical engineering. Improving effective microsystem cooling designs is central to these initiatives. One subset of nanomaterials, nanofluids have stimulated substantial attention. Nanofluids [**1**] achieve demonstrably greater effective thermal conductivities and convective heat transfer coefficients as compared with conventional base fluids (e.g. air and water). Nanofluids are synthesized by suspending nanoparticles which may be metallic (*Al, Cu, Al_2 O_3, SiC, AlN, SiN)* or non-metallic (graphite, carbon nanotubes) in base fluids. Applications of nanofluids are growing in increasingly rich and diverse technologies including anti-bacterial systems, cancer therapy, solar cell

enhancement and coolants for propulsion and lubrication designs [**2-5**]. Nanofluid convective heat transfer and other thermal characteristics have been recently reviewed by Tripathi and Bég **[6]** for application in pharmacology, Kleinstreuer and Xu **[7]** for microchannels**,** Sadeghi *et al.* **[8]** for circular tubes fitted with helical inserts, Vajjha *et al*. **[9]** for turbulent flows, Shin and Banerjee [**10**] for nano-materials processing, Huminic and Huminic **[11]** for curve tube and Mahian *et al*. **[12]** for entropy generation minimization. Numerous numerical and theoretical studies of nanofluid transport have also been communicated which have elaborated in detail the improved thermal performance achieved with such fluids. Rana *et al*. [**13**] employed a finite element algorithm to investigate nonlinear viscoelastic nanofluid flow from an extending sheet with deformation effects. Tripathi *et al.* **[14]** studied analytically the transient peristaltic diffusion of nanofluids in tapered channels. Basir *et al.* [**15**] examined multiple slip effects in nanofluid enrobing flow from an extending cylindrical body with Maple software. Hamad and Ferdows [**16**] studied heat sink/source and wall transpiration effects on stagnation point nanofluid flow from a stretching sheet. Akbar *et al.* [**17**] addressed theoretically the cilia-driven propulsion of CNT nanofluids in porous media with entropy generation effects. *Magnetic nanofluids* have also drawn significant interest in applied mathematical modelling in recent years. In such flows the nano-particles response to the imposition of externally imposed magnetic fields and the nanofluids are electrically-conducting [**18**]. Representative studies of magnetohydrodynamic nanofluid simulation include Noreen *et al.* **[19]** who studied magnetic nanofluid peristaltic flow in a curved channel with induction effects. Bég *et al.* [**20**] used the Tiwari-Das nanofluid model to study Marangoni-driven hydromagnetic non-isothermal nanofluid flow, examining silver, copper, aluminium oxide and titanium oxide nano-particles and also considering magnetic induction effects. They observed that the flow and magnetic induction function are depressed with greater nanofluid solid volume fraction, whereas temperatures are increased. Akbar *et al*. **[21]** investigated the magnetic peristaltic transport of carbon nanotube nanofluids in a permeable channel, specifically addressing induction and heat flux effects. Shehzad *et al.* [**22**] evaluated the influence of boundary convective heat and concentration conditions in magnetohydrodynamic flow of non-Newtonian nanofluids, observing that temperature and nanoparticle concentrations are increased with greater Biot numbers whereas the flow is retarded with greater magnetic field.

A special sub-category of boundary layer flows known as “Sakiadis flows” [**23**] are concerned with transport from a stretching surface. This type of flow is fundamental to materials processing systems, chemical and process engineering operations (polymer synthesis). Consequently a wide variety of problems dealing with heat and fluid flow over a stretching sheet have been studied with

both Newtonian and non-Newtonian fluids with applications in extrusion, melt-spinning, hot rolling, wire drawing, glass- fiber production, manufacture of plastic and rubber sheets, cooling of a large metallic plate in a bath and so on. Gupta and Gupta **[24]** considered the case where the stretching sheet is subjected to a constant mass flux and emphasized that a stretching sheet may not always conform to the linear speed assumed by them. Wang **[25]** reported the flow caused by the stretching of a flat surface in two lateral directions. Char and Chen **[26]** extended their problem for non-Newtonian flow. Nadeem ***et al***. **[27]** investigated the three dimensional viscous flow of Casson fluids over the stretching sheet. Cortell **[28]** further extended the boundary layer flow of viscoelastic fluids with heat generation and absorption. Nadeem *et al*. **[29**] obtained numerical solutions for the boundary layer flow of Maxwell fluids over a stretching sheet. Bhargava *et al.* [**30**] computed finite element solutions for micropolar stretching sheet flow. Many other investigations have been communicated on boundary layer flow of Newtonian and non-Newtonian fluids with heat transfer effects and without it over a stretching sheet. With regard to nanofluids, extensive research has also been conducted recently to consider stretching sheet flow scenarios. The improved performance and sustainability of nanofluids requires deeper understanding of their manufacturing processes in order to manipulate characteristics for specific applications. Stretching sheet flows frequently arise in such manufacturing processes and magnetohydrodynamics (MHD) is often deployed to better control heat and mass characteristics of nanomaterials. Recent studies in this regard include the articles by Khan and Pop [**31**] and Makinde and Aziz [**32**]. Bég *et al*. [**33**] used a finite difference technique to computationally study the more complex scenario of transient magnetic nanofluid free and forced convection boundary layers from an exponentially extending sheet in permeable media. Rana and Bhargava [**34**] used a variational finite element code to simulate heat and mass transfer in nanofluids from a non-linear stretching sheet. Further studies include Hamad [**35**], Uddin *et al*. [**36**] who considered also a shrinking sheet and Navier slip, Khan *et al.* [**37**] who examined oblique magnetized radiative stagnation point stretching sheet flow, Uddin *et al.* [**38**], Mabood *et al.* [**39**] and Uddin *et al*. [**40**]. These analyses all confirmed the thermally-enhancing properties of nanofluids.

The above studies have generally neglected viscosity variation in nanofluids, a feature that may be of critical importance in materials processing. In the present article, we therefore consider *magnetohydrodynamic boundary layer convection of temperature-dependent viscous nanofluids controlled from a stretching sheet with multiple (thermal and species) buoyancy effects*. An efficient numerical technique, Runge–Kutta fourth order quadrature [**41**] is employed to determine numerical solutions for the dimensionless boundary value problem. Verification of the solutions is achieved

with the Nakamura tridiagonal finite difference method [**42**]. The influence of key nanoscale, magnetic, geometric and thermofluid parameters on the heat, momentum and mass transfer characteristics is evaluated.

2. MATHEMATICAL MAGNETIC VARIABLE-VISCOSITY NANOFLUID MODEL

The regime under investigation is illustrated in **Fig. 1**. Two-dimensional, steady-state, incompressible flow of an electrically-conducting nanofluid from a vertical stretching sheet is considered, with reference to an (*x*,*y*) coordinate system, where the *x*-axis is aligned with the sheet. A transverse static uniform strength magnetic field is applied, which is sufficiently weak to negate magnetic induction and Hall current effects. The nanofluid is dilute and comprises a homogenous suspension of equally-sized nanoparticles in thermal equilibrium. The sheet is stretched in the plane $y = 0$. The flow is assumed to be confined to $y > 0$. Here we assumed that the sheet is uniformly extended with the linear velocity $u(x) = ax$, where $a > 0$ is constant and the *x*-axis is measured along the stretching surface. Under these assumptions, the governing conservation equations for mass, momentum, energy (heat) and nano-particle species diffusion (concentration) conservation, neglecting viscous and Joule dissipation effects, may be shown to take the form:

$$\frac{\partial u}{\partial x} + \frac{\partial v}{\partial y} = 0, \tag{1}$$

$$\rho\left(u\frac{\partial u}{\partial x} + v\frac{\partial u}{\partial y} \right) = \frac{\partial}{\partial y}\left(\mu(T)\frac{\partial u}{\partial y} \right) - \sigma B_o^2 u + \rho g\beta_T (T - T_\infty) + \rho g\beta_C (C - C_\infty), \tag{2}$$

$$\left(\rho c_p\right)\left(u\frac{\partial T}{\partial x} + v\frac{\partial T}{\partial y} \right) = k\frac{\partial^2 T}{\partial y^2} + \tau\left[D_B\frac{\partial T}{\partial y}\frac{\partial C}{\partial y} + \left(\frac{D_T}{T_\infty}\right)\left(\frac{\partial T}{\partial y}\right)^2 \right], \tag{3}$$

$$\left(u\frac{\partial \phi}{\partial x} + v\frac{\partial \phi}{\partial y} \right) = D_B\frac{\partial^2 C}{\partial y^2} + \left(\frac{D_T}{T_\infty}\right)\frac{\partial^2 T}{\partial y^2}. \tag{4}$$

Here $\tau = \dfrac{(\rho c)_p}{(\rho c)_f}$ denotes the ratio of the effective heat capacity of the nano-particles to the base fluid, *u* and *v* are the velocity components along the *x* and *y*-directions respectively, *T* is the temperature of the magnetic nanofluid, C is the nano-particle concentration, B_0 is the magnitude of magnetic field strength.

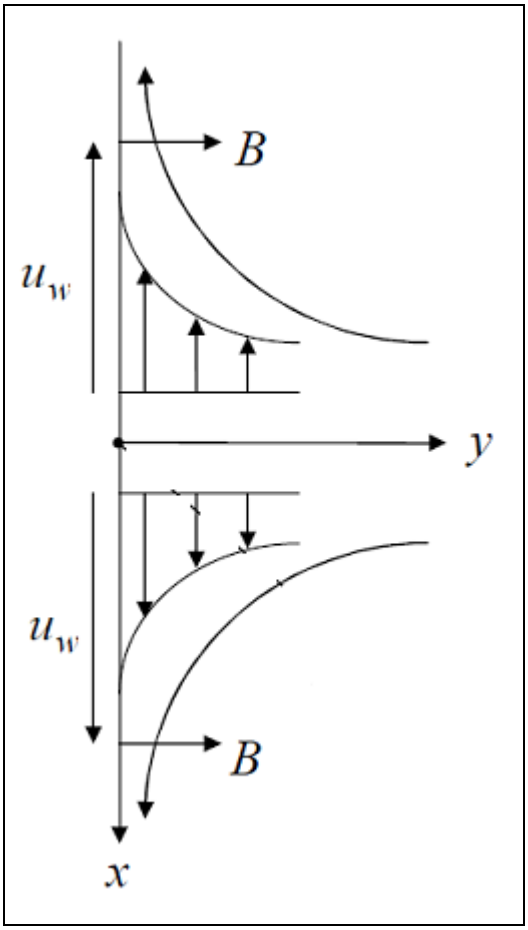

Fig.1. Physical model for magnetohydrodynamic nanofluid stretching sheet problem.

The boundary conditions are prescribed as follows:

$$u = u_w(x) = ax, \quad v = 0, \quad T = T_w, \quad C = C_w, \text{ at y = 0,} \tag{5}$$

$$u \to 0, \quad v \to 0, \quad T \to T_\infty, \quad C \to C_\infty, \text{ as } y \to \infty. \tag{6}$$

To facilitate numerical solutions to the primitive boundary value problem, it is pertinent to introduce the following similarity transformations and dimensionless variables:

$$u = axf'(\eta), \; v = -\sqrt{(a\nu)}f(\eta), \; \eta = \sqrt{\left(\frac{a}{\nu}\right)}y, \; \theta(\eta) = \frac{T - T_\infty}{T_w - T_\infty}, \; \phi(\eta) = \frac{C - C_\infty}{C_w - C_\infty}, \tag{7}$$

To simulate temperature-dependent viscosity variation, we adopt the robust Reynolds exponential viscosity model [**43**] which provides an accurate approach:

$$\mu(\theta) = e^{-(\alpha\theta)} = 1 - (\alpha\theta) + O(\alpha^2), \tag{8}$$

where α is the viscosity parameter.

Implementing eqns. (7, 8) in the conservation eqns. (1) to (6), the following nonlinear, coupled system of self-similar ordinary differential equations emerges:

$$(1-(\alpha\theta))\,f'''-\alpha\theta' f''-(f')^2+ff''-M^2 f'+G_r\theta+B_r\phi=0, \tag{9}$$

$$\frac{1}{\Pr}\theta''+f\theta'+N_b\theta'\xi'+N_t(\theta')^2=0, \tag{10}$$

$$\phi''+Scf\phi'+\frac{N_t}{N_b}\theta''=0, \tag{11}$$

The transformed boundary conditions assume the form:

$$\left.\begin{aligned} &f(0)=0,\quad f'(0)=1,\ \ \theta(0)=1,\ \ \phi(0)=1, && \text{(12a)}\\ &f'(\infty)=0,\quad \theta(\infty)=0,\ \ \phi(\infty)=0, && \text{(12b)}\end{aligned}\right\}$$

where primes denote differentiation with respect to η i.e. the transformed transverse coordinate. Furthermore the following dimensionless numbers invoked in eqns. (9)-(11) are defined as follows:

$$\left.\begin{aligned} &M^2=\frac{\sigma {B_0}^2}{\rho\, a},\quad R_{ex}=\frac{u_w(x)x}{\nu},\ G_T=\frac{\rho g x^3\beta_T(T_w-T_\infty)}{\nu^2},\ G_r=\frac{G_T}{{R_{ex}}^2},\\ &\Pr=\frac{\nu}{\alpha},\ N_b=\frac{\tau D_B(\phi_w-\phi_\infty)}{\nu},\ N_t=\frac{\tau D_T(T_w-T_\infty)}{\nu T_\infty},\quad Sc=PrLe,,\\ &B_T=\frac{\rho g x^3\beta_C(C_w-C_\infty)}{\nu^2},\ B_r=\frac{B_T}{{R_{ex}}^2}.\end{aligned}\right\} \tag{13}$$

These represent respectively the square of the *Hartmann magnetic body force number, local Reynolds number, local thermal Grashof number* (ratio of *thermal buoyancy force* to *viscous force) thermal buoyancy ratio parameter, Prandtl number, Brownian motion parameter, thermophoresis parameter, Schmidt number (defined as the product of Prandtl and Lewis numbers), local solutal (species) Grashof number* (ratio of *nano-particle concentration buoyancy force* to *viscous force*), and *species buoyancy ratio parameter*. Expressions for the skin friction coefficient (wall shear stress function), local Nusselt number (wall heat transfer rate) and the local Sherwood number (wall nano-particle mass transfer rate) may also be defined as follows:

$$c_f=\frac{\tau_w}{\rho {u_w}^2},\quad Nu_x=\frac{-xq_m}{\alpha_1(T_w-T_\infty)},\quad Sh_x=\frac{-xq_m}{\alpha_1(C_w-C_\infty)}, \tag{14}$$

$$\tau_w=\mu(T)\left(\frac{\partial u}{\partial y}\right),\quad q_w=-\alpha_1\left(\frac{\partial T}{\partial y}\right),\qquad q_m=-\alpha_1\left(\frac{\partial C}{\partial y}\right), \tag{15}$$

$$(\mathrm{Re}_x)^{1/2}c_f=(1-(\alpha\theta(0)))\,f''(0),\ \ (\mathrm{Re}_x)^{1/2}Nu_x=-\theta'(0)\ \mathrm{Re}_x^{-\frac{1}{2}}Sh_x=-\phi'(0), \tag{16}$$

3. NUMERICAL SOLUTIONS OF TRANSFORMED EQUATIONS AND VALIDATION

The nonlinear ordinary differential equations (9)-(11) subject to the boundary conditions (12a & 12b) have been solve numerically using an efficient Runge–Kutta (RK) fourth order method along with a shooting technique. The asymptotic boundary conditions given by Eq. (12) were replaced by using a value of 15 for the similarity variable $\eta_{\max}$. The choice of $\eta_{\max} = 15$ and the step size $\Delta\eta = 0.001$, ensured that all numerical solutions approached the asymptotic values correctly. The methodology of the RK algorithm is well-documented and readers are referred to, for example Bég and Makinde [**44**]. To verify the general model presented in the previous section, it is necessary to resolve the two point boundary problem defined by Eqns. (9) – (11) under boundary conditions (12a, b) with an alternative procedure. Although benchmarking for special cases is possible with literature, these do not validate the general case. This furthermore provides researchers with a complete set of solutions against which they can validate extensions of the present model. We employ a second order accurate finite difference algorithm known as Nakamura's method to validate the general RK solutions. The Nakamura tridiagonal method [**45**] generally achieves fast convergence for nonlinear viscous flows which may be described by either parabolic (boundary layer) or elliptic (Navier-Stokes) equations. **The coupled 7**th order system of nonlinear, multi-degree, ordinary differential equations defined by (9)–(11) with boundary conditions (12a,b) is solved using the NANONAK code in double precision arithmetic in Fortran 90, as elaborated by Bég [**46**]. Computations are performed on an SGI Octane Desk workstation with dual processors and take seconds for compilation. As with other difference schemes, a reduction in the higher order differential equations, is also fundamental to **Nakamura's method**. The method has been employed successfully to simulate many sophisticated nonlinear transport phenomena problems e.g. magnetized bio-rheological coating flows (Bég *et al.* [**47]**). Intrinsic to this method is the discretization of the flow regime using an equi-spaced finite difference mesh in the transformed coordinate (η). The partial derivatives for f, θ, ϕ with respect to η are evaluated by central difference approximations. An iteration loop based on the *method of successive substitution* is utilized to advance the solution i.e. march along the domain. The finite difference discretized equations are solved in a step-by-step fashion on the η-domain. For the energy and nano-particle species conservation Eqns. (10) - (11) which are *second order* multi-degree ordinary differential equations, only a *direct substitution* is needed. However a reduction is required for the *third order* momentum Eqn. (9). We apply the following substitutions:

$$P = f' \tag{17}$$

$$Q = \theta \tag{18}$$

$$R = \phi \tag{19}$$

The ODEs (9)-(11) then retract to:

Nakamura momentum equation:

$$A_1 P^{//} + B_1 P^{/} + C_1 P = T_1 \tag{20}$$

Nakamura energy equation:

$$A_2 Q^{//} + B_2 Q^{/} + C_2 Q = T_2 \tag{21}$$

Nakamura nano-particle species equation:

$$A_3 R^{//} + B_3 R^{/} + C_3 R = T_3 \tag{22}$$

Here A_i*=1,2,3,* B_i*=1,2,3,* C_i*=1,2,3* are the Nakamura matrix coefficients, T_i*=1,2,3* are the Nakamura source terms containing a mixture of variables and derivatives associated with the respective lead variable (*P*, *Q*, *R*). The Nakamura Eqns. (20)–(22) are transformed to finite difference equations and these are orchestrated to form a tridiagonal system which due to the high nonlinearity of the numerous coupled, multi-degree terms in the momentum, energy, nano-particle species conservation equations, is solved *iteratively*. Householder's technique is ideal for this iteration. The boundary conditions (12) are also easily transformed. The iterative process is assumed to attain a convergent solution when the following condition is satisfied (Θ denotes a general variable, *n* and *n-1* are adjacent nodes):

$$\sum_i \left| \Theta_i^n - \Theta_i^{n-1} \right| \leq 10^{-6} \tag{23}$$

Further details of the **NTM** approach are provided in Nakamura [**48**] and Bég [**49**]. Comparisons with the RK quadrature solutions are documented in **Tables 1-4** for skin friction i.e. $(\mathrm{Re}_x)^{1/2} c_f = (1-(\alpha\theta(0)))\, f''(0)$ and Nusselt number i.e. wall heat transfer rate, $(\mathrm{Re}_x)^{1/2} Nu_x = -\theta'(0)$, respectively. Generally very close correlation is obtained between RK shooting quadrature (RK) and the Nakamura finite difference (NFD) method over a range of magnetic (*M*), thermal Grashof number (*Gr*) and species Grashof numbers (*Br*). Confidence in the RK45 numerical solutions is therefore justifiably high. In **section 4** all graphical plots are generated with RK numerical quadrature solutions. **Table 1** indicates that for the non-magnetic case (*M* = 0), with increasing thermal Grashof number the skin friction is reduced whereas with increasing species Grashof number it is enhanced.

Table 1: Numerical values of skin friction computed with RK and NFD methods with various values of α , *Br and Gr* with *M= 0, Nb = Nt = 0.5, Sc = 10 and Pr =3.97.*

$\alpha\downarrow$	*M= 0 (non-conducting nanofluid case)*							
	Br = 0				*Br* = 0.5			
	Gr=0.5 RK	*Gr*=0.5 NFD	*Gr*=1 RK	*Gr=1* NFD	*Gr*=0.5 RK	*Gr*=0.5 NFD	*Gr*=1 RK	*Gr=1* NFD
0	0.80274	0.80275	0.61617	0.61612	0.80523	0.80532	0.62035	0.62049
0.1	0.76906	0.76910	0.58613	0.58619	0.77175	0.77184	0.59055	0.59063
0.2	0.73275	0.73278	0.55398	0.55401	0.73566	0.73572	0.55867	0.55874
0.3	0.69327	0.69330	0.51932	0.51951	0.69644	0.69651	0.52432	0.52439
0.4	0.64993	0.64996	0.48167	0.48181	0.65343	0.65361	0.48701	0.48717
0.5	0.60174	0.60171	0.44032	0.44039	0.60563	0.60580	0.44605	0.44613

Table 2: Numerical values of skin friction computed with RK and NFD methods with various values of α , *Br and Gr* with *M= 1, Nb = Nt = 0.5, Sc = 10 and Pr =3.97.*

$\alpha\downarrow$	*M = 1*							
	Br = 0				*Br* = 0.5			
	Gr=0.5 RK	*Gr*=0.5 NFD	*Gr*=1 RK	*Gr=1* NFD	*Gr*=0.5 RK	*Gr*=0.5 NFD	*Gr*=1 RK	*Gr=1* NFD
0	1.22381	1.22388	1.04349	1.04352	1.22531	1.22541	1.04681	1.04676
0.1	1.17163	1.17170	0.99543	0.99555	1.17336	1.17344	0.99903	0.99911
0.2	1.11540	1.11552	0.94391	0.94387	1.11742	1.11737	0.94784	0.94789
0.3	1.05434	1.05448	0.88831	0.88828	1.05671	1.05669	0.89261	0.89258
0.4	0.98739	0.98743	0.82778	0.82782	0.99018	0.99022	0.83250	0.83246
0.5	0.91303	0.91310	0.76112	0.76109	0.91635	0.91631	0.76633	0.76629

Table 3: Numerical values of Nusselt number computed with RK and NFD methods with various values of α , *Br and Gr* with *M= 0, Nb = Nt = 0.5, Sc = 10 and Pr =3.97*.

$\alpha\downarrow$	*M = 0 (non-conducting nanofluid case)*							
	Br = 0				*Br* = 0.5			
	Gr=0.5 RK	*Gr*=0.5 NFD	*Gr*=1 RK	*Gr=1* NFD	*Gr*=0.5 RK	*Gr*=0.5 NFD	*Gr*=1 RK	*Gr=1* NFD
0	0.96537	0.96539	0.99031	0.99035	0.96880	0.96877	0.99313	0.99321
0.1	0.95834	0.95840	0.98510	0.98516	0.96203	0.96211	0.98809	0.98813
0.2	0.95045	0.95049	0.97934	0.97937	0.95444	0.95435	0.98251	0.98257
0.3	0.94150	0.94155	0.97289	0.97294	0.94583	0.94589	0.97628	0.97622
0.4	0.93119	0.93123	0.96561	0.96564	0.93594	0.93599	0.96924	0.96933
0.5	0.91910	0.91914	0.95725	0.95727	0.92436	0.92429	0.96116	0.96124

Table 4: Numerical values of Nusselt number computed with RK and NFD methods with various values of α , *Br and Gr* with *M= 1, Nb = Nt = 0.5, Sc = 10 and Pr =3.97*.

$\alpha\downarrow$	*M = 1*							
	Br = 0				*Br* = 0.5			
	Gr=0.5 RK	*Gr*=0.5 NFD	*Gr*=1 RK	*Gr=1* NFD	*Gr*=0.5 RK	*Gr*=0.5 NFD	*Gr*=1 RK	*Gr=1* NFD
0	0.88976	0.88982	0.91824	0.91831	0.89405	0.89409	0.92169	0.92176
0.1	0.87954	0.87959	0.91023	0.91030	0.88418	0.88423	0.91390	0.91393
0.2	0.86806	0.86798	0.90132	0.90138	0.87311	0.87314	0.90525	0.90532
0.3	0.85501	0.85494	0.89134	0.89139	0.86054	0.86047	0.89555	0.89561
0.4	0.83997	0.83988	0.88000	0.88002	0.84608	0.84612	0.88454	0.88449
0.5	0.82234	0.82228	0.86694	0.86687	0.82915	0.82921	0.87185	0.87179

Table 2 shows that with magnetic body force present (M = 1 implies viscous and magnetic drag forces are equal), increasing thermal Grashof number strongly reduces the skin friction whereas increasing species Grashof number weakly increases skin friction. **Tables 3** and **4** show that for both the non-magnetic (M = 0) and (M = 1) magnetic cases, Nusselt number is increased with both increasing thermal Grashof number increasing species Grashof number it is enhanced. However thermal Grashof number exerts a more significant impact than species Grashof number.

4. RESULTS AND DISCUSSION

Extensive graphical plots obtained with RK quadrature are presented in **Figs. 2-10**, for the variation of velocity, temperature, nano-particle concentration, skin friction coefficient, Nusselt number and streamline distributions with selected thermophysical parameters.

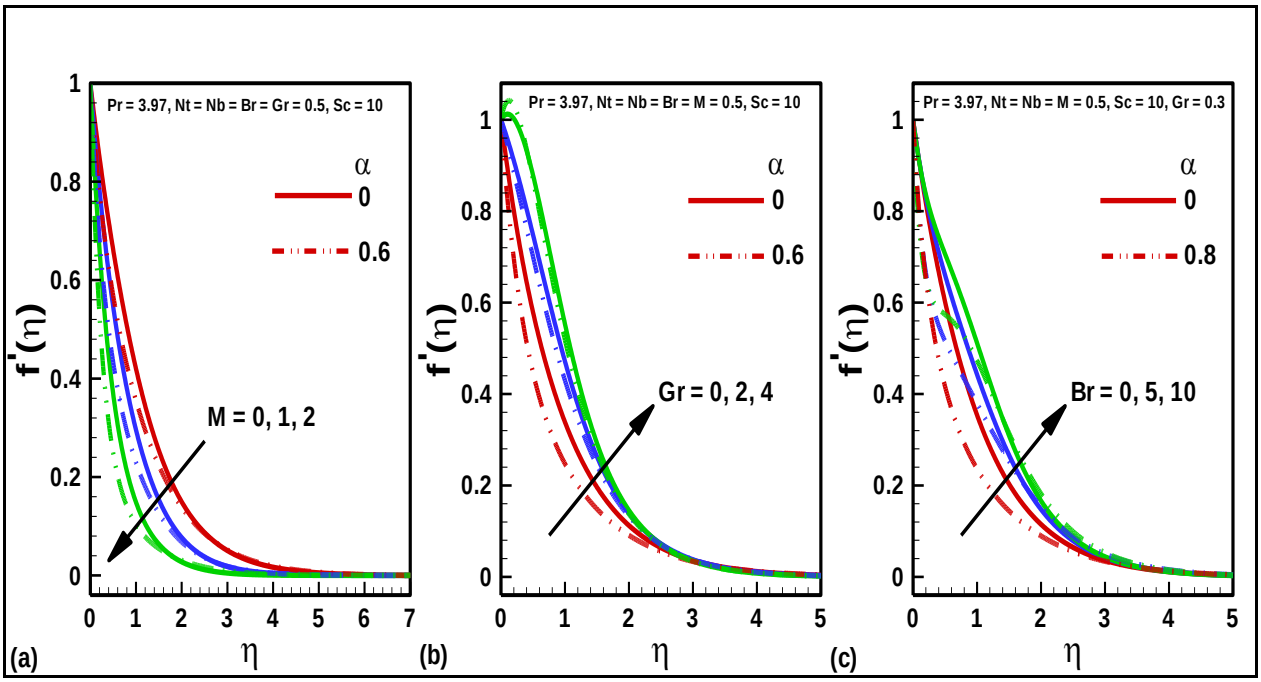

Fig.2. Velocity profile for constant and variable viscosity cases with variation of **(a)** Hartmann number (M) **(b)** Thermal Grashof number (Gr) **(c)** Concentration Grashof number (Br).

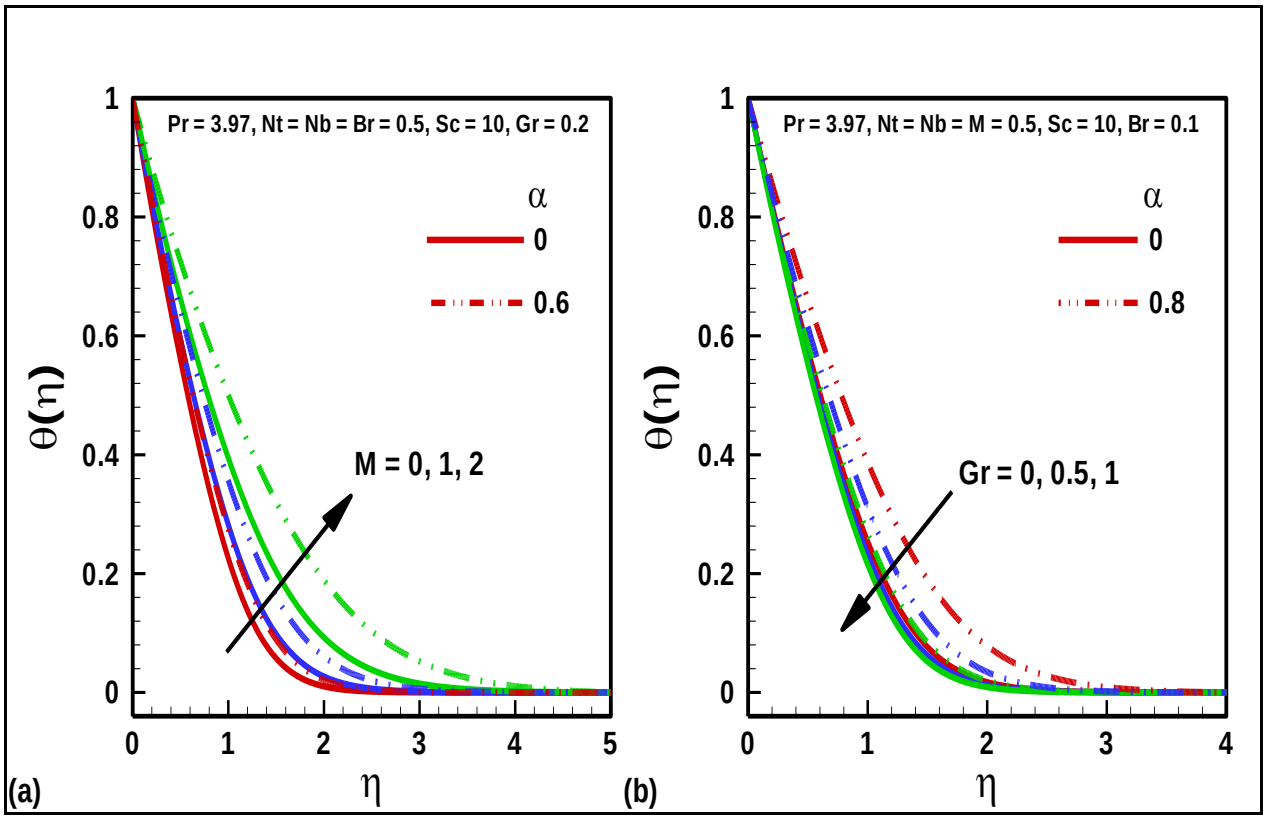

Fig.3. Temperature profile for constant and variable viscosity cases with variation of **(a)** Hartmann number (*M*) **(b)** Thermal Grashof number (*Gr*).

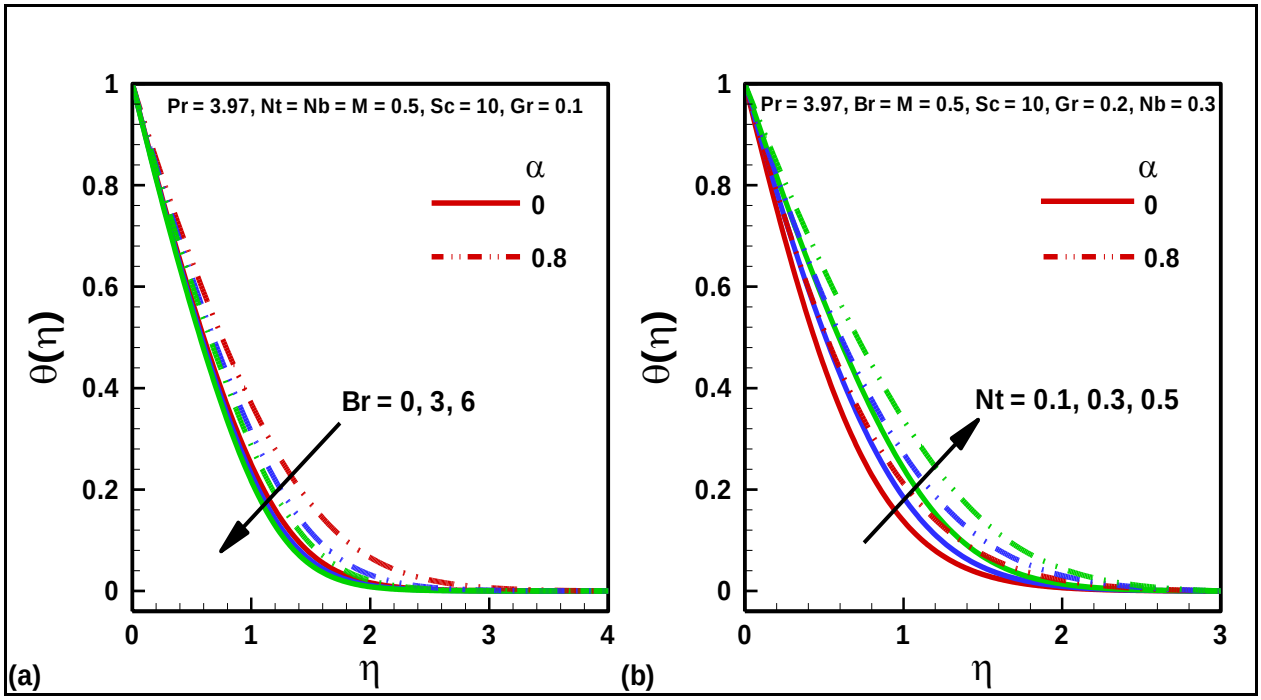

Figs.4. Temperature profile for constant and variable viscosity cases with variation of **(a)** Concentration Grashof number (*Br*) **(b)** Thermophoresis parameter (*Nt*).

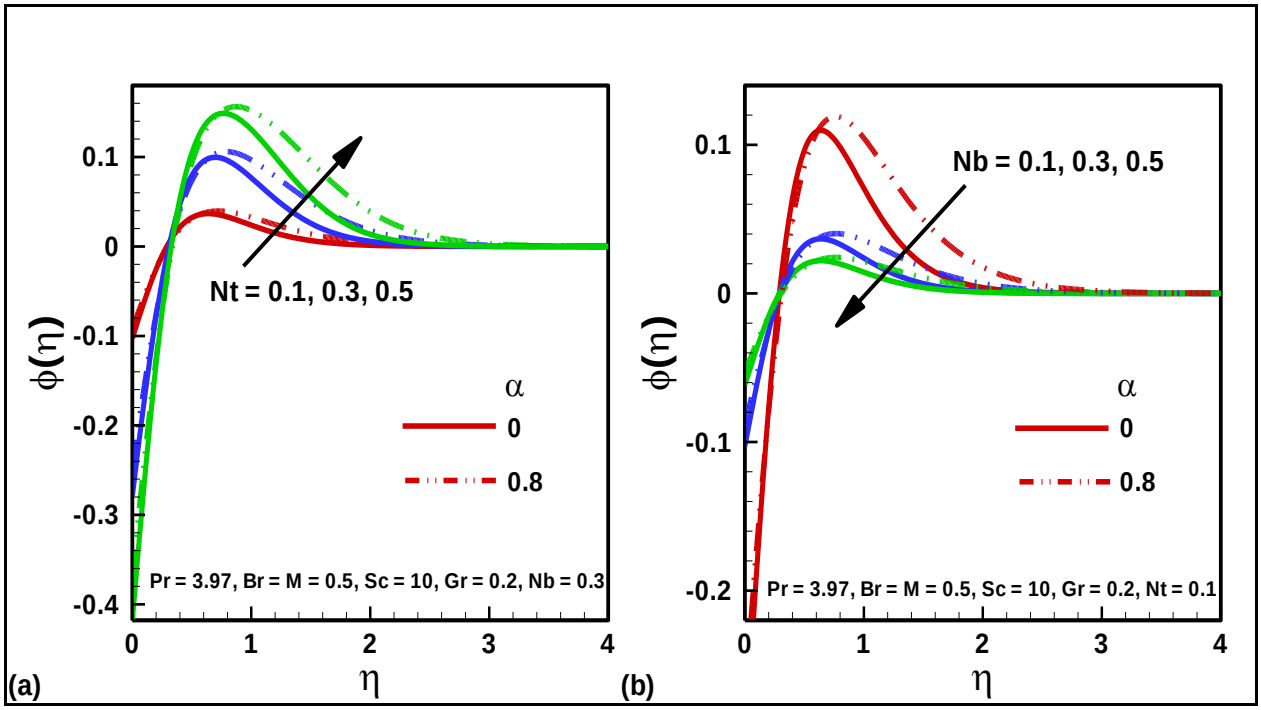

Fig.5. Concentration profile for constant and variable viscosity cases with variation of **(a)** Thermophoresis parameter (*Nt*) **(b)** Brownian motion parameter (*Nb*).

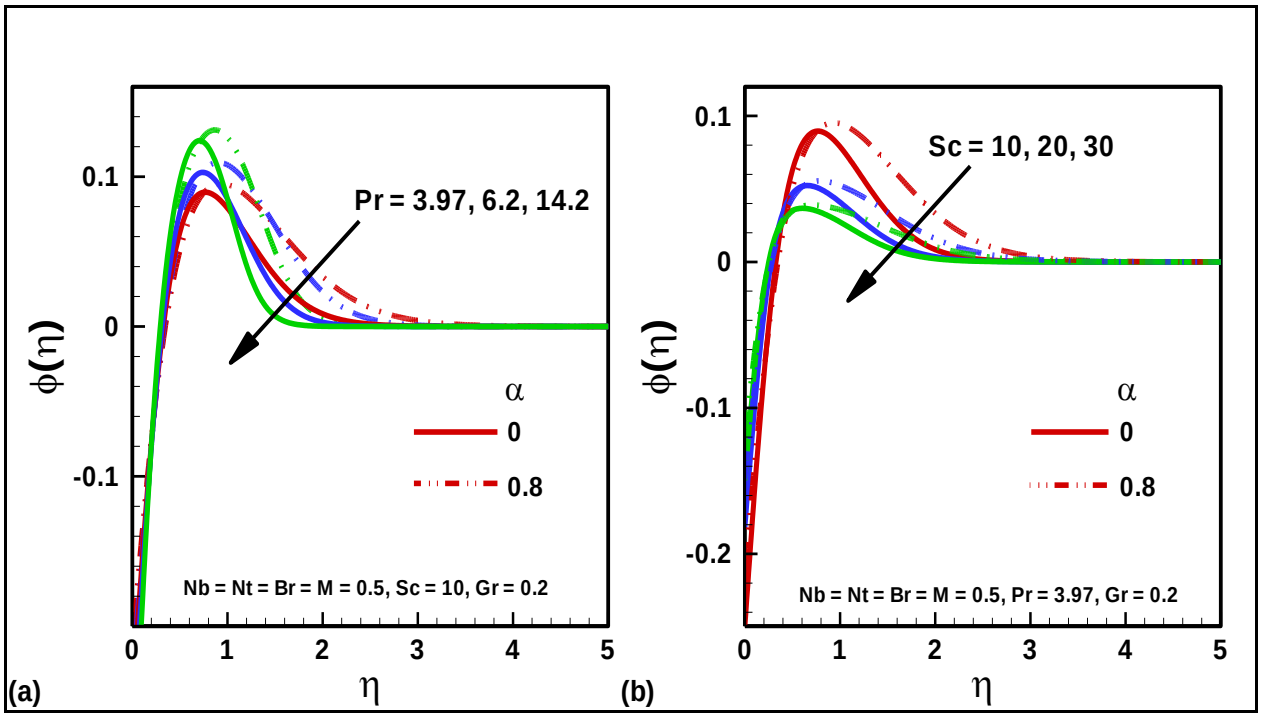

Fig.6. Concentration profile for constant and variable viscosity cases with variation of **(a)** Prandtl number (*Pr*) **(b)** Schmidt number (*Sc*).

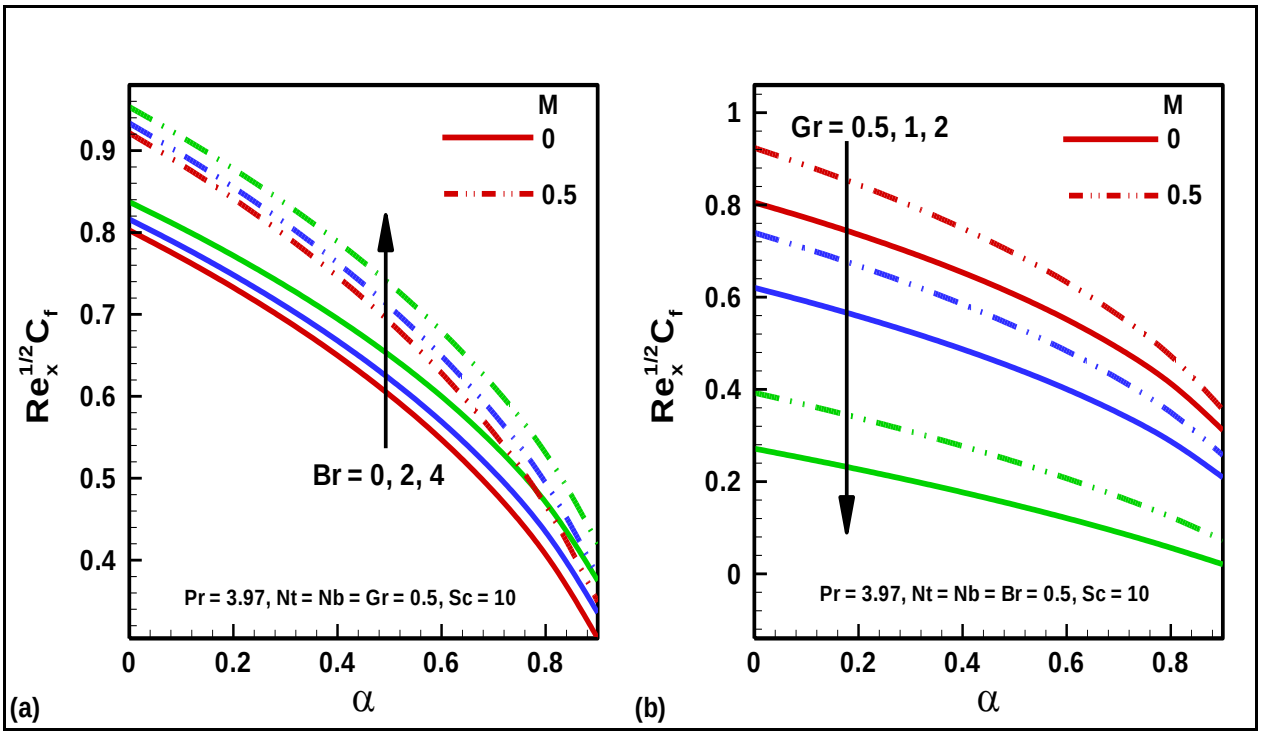

Fig.7. Skin Friction coefficient with variation of **(a)** Solutal (concentration) Grashof number (*Br*) **(b)** Thermal Grashof number (*Gr*).

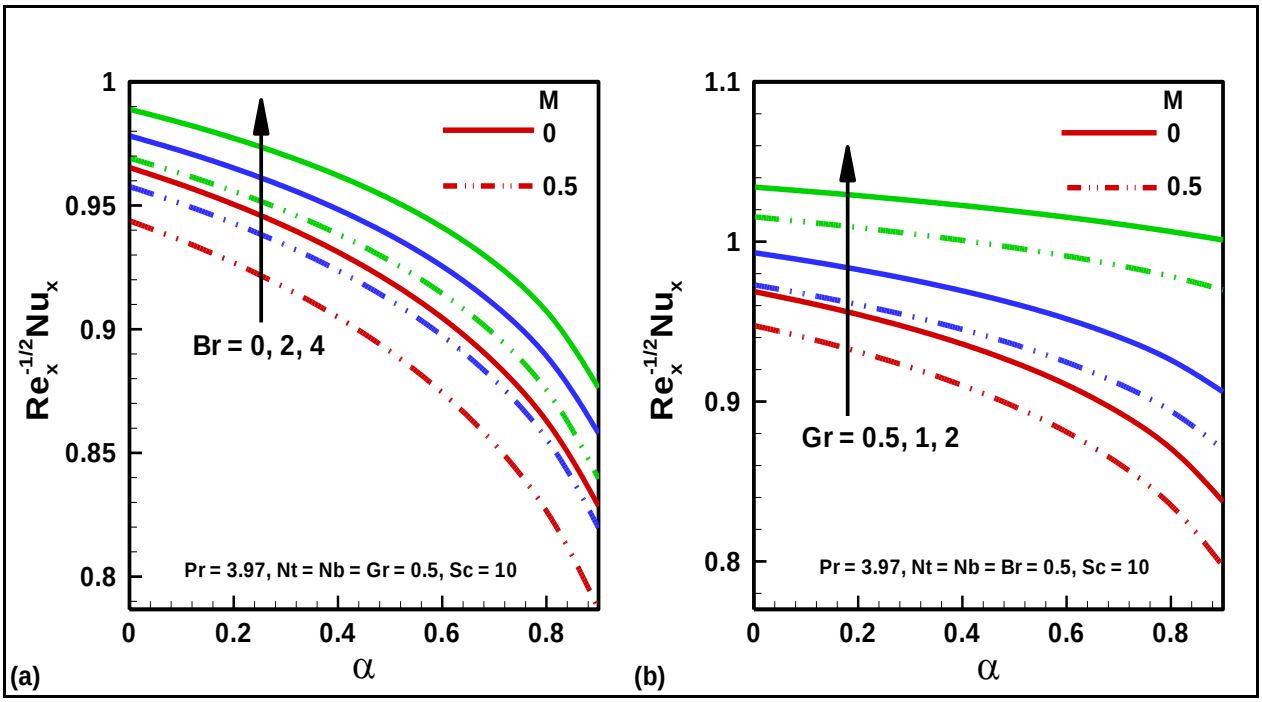

Fig.8. Nusselt number with variation of **(a)** Solutal (concentration) Grashof number (*Br*) **(b)** Thermal Grashof number (*Gr*).

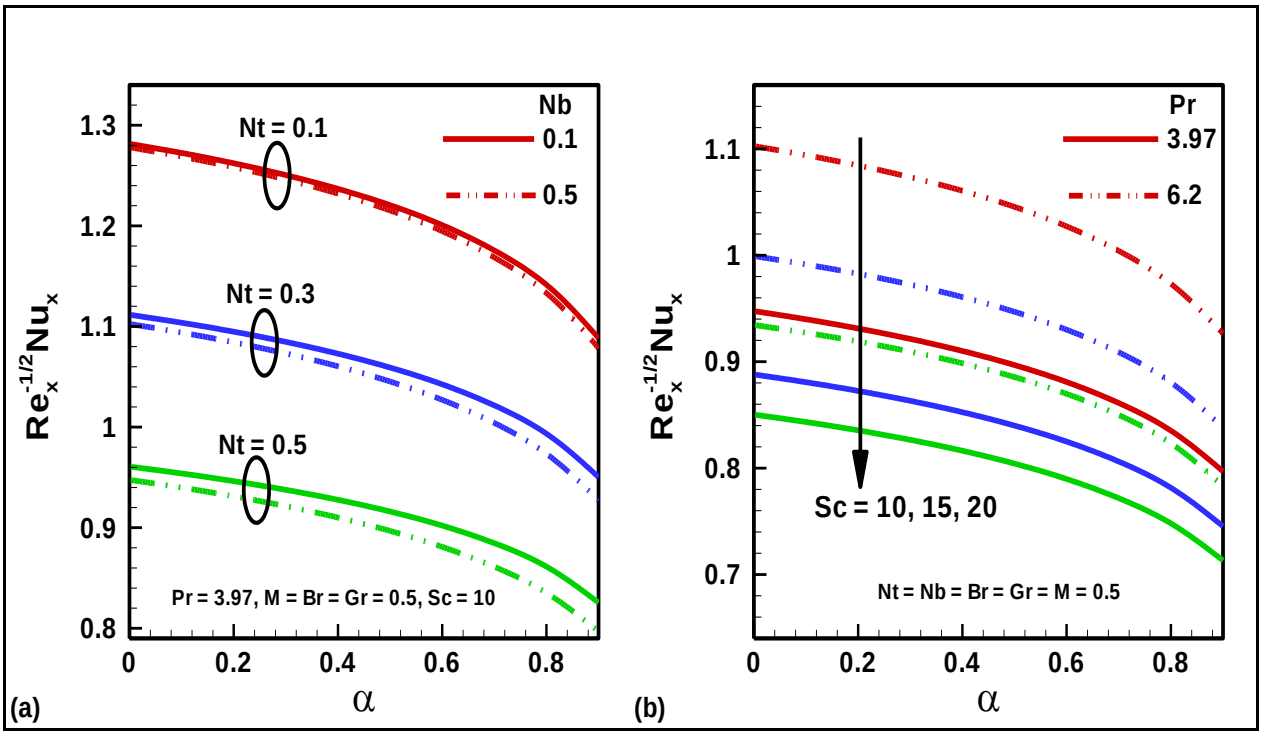

Fig.9. Nusselt number with variation of **(a)** Thermophoresis parameter (*Nt*) **(b)** Schmidt number (*Sc*).

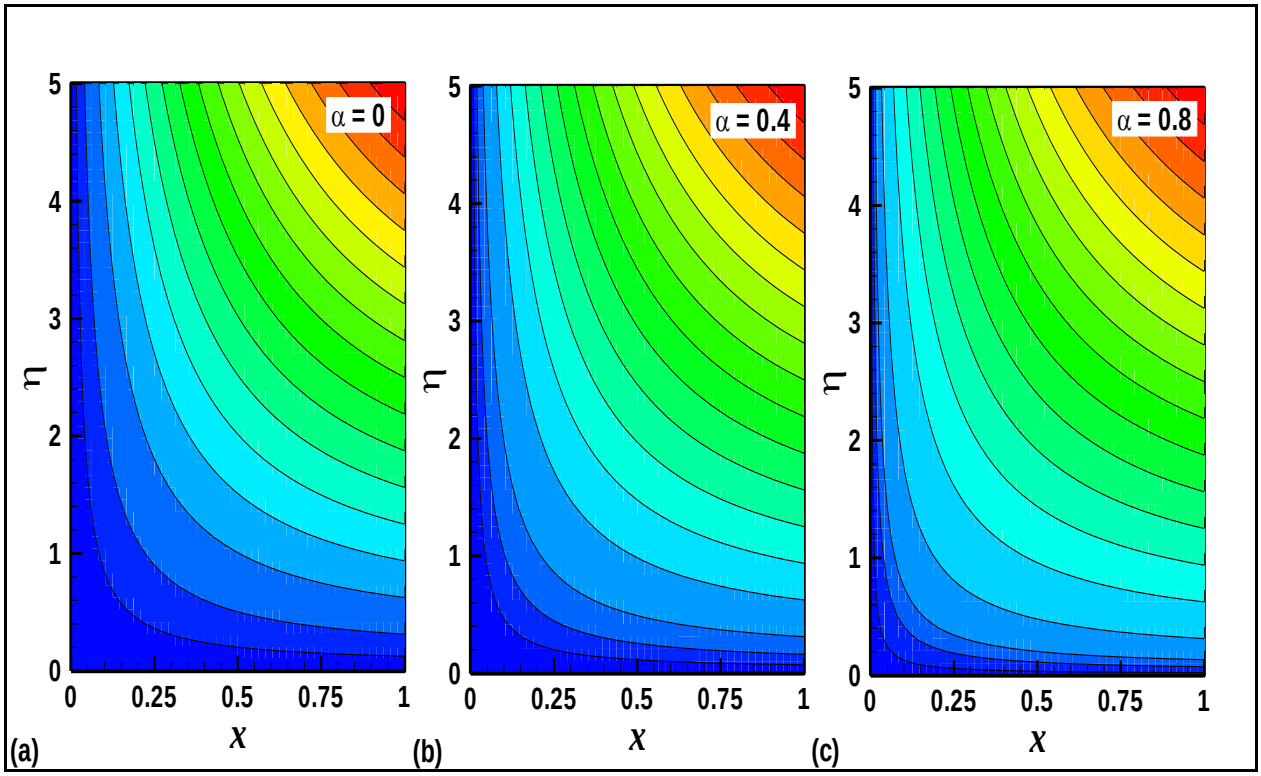

Figs.10. Streamline plots with the variation of viscosity parameter (α).

Figs. 2(a-c) shows the variation of axial velocity against the transverse coordinate under the effects of Hartmann number, thermal Grashof number and species Grashof number. It is observed that the velocity profile is nonlinear (monotonic decay) and attains a maximum at the origin ($\eta = 0$). All profiles descend smoothly to vanishing values in the free stream. In fig.2a, the influence of Hartmann number on velocity magnitudes is depicted for two different values of viscous parameter $\alpha = 0$ (plotted as solid lines) and $\alpha = 0.6$ (plotted as dotted lines). The former case implies constant viscosity i.e. no variation and the latter is associated with exponential viscosity increase. Velocity diminishes with increasing the magnitude of viscous parameter. This is attributable to the increase in viscous force relative to inertial forces with greater viscosity which decelerates the flow. Momentum boundary layer thickness will therefore be increased. Similarly the flow is retarded i.e. velocity magnitudes are reduced with increasing the effect of magnetic field. The Lorentzian magneto-hydrodynamic component in the momentum eqn. (9), i.e.-$M^2 f'$ is a drag force which acts in the negative axial direction transverse to the line of application which is in the positive transverse direction. With greater Hartmann number, *M*, the magnetic field strength is also increased. This inhibits the flow and also enhances momentum boundary layer thickness in the stretching nanofluid sheet. These results concur with other studies e.g. Gorla *et al*. [**50**]. Flow control is therefore successfully achieved with the imposition of a transverse magnetic field. However flow reversal is never generated anywhere in the boundary layer since velocity magnitudes are consistently positive. In fig.2b, the effect of thermal Grashof number (*Gr*) on velocity profile is illustrated and it is evident that velocity is enhanced with increasing *Gr* values. For *Gr* = 0 thermal buoyancy force is negated i.e. $Gr\theta \rightarrow 0$ in eqn. (9). For *Gr* = *2*, *4* the thermal buoyancy force is progressively increased relative to the viscous hydrodynamic force. For *Gr* = 4 a velocity overshoot arises near the wall which is absent for lower thermal Grashof numbers. This aids in momentum development in the boundary layer and accelerates the flow also leading to a decrease in momentum (hydrodynamic) boundary layer thickness. Again an increase in viscosity parameter induces the opposite effect and decelerates the flow and increases momentum boundary layer thickness. In fig.2c, the effect of increasing species (solutal) Grashof number, *Br*, is also to enhance the velocity magnitudes i.e. to accelerate the flow and decrease momentum boundary layer thickness. For *Br* = 0 the nano-particle species buoyancy force in eqn. (9) vanishes i.e. $Br\phi \rightarrow 0$. For any non-zero value of *Br* studied i.e. 5, 10, however there is *never any velocity overshoot present* as with the thermal Grashof number (fig. 2b).

Figures 3 & 4 depicts the evolution in temperature function, $\theta(\eta)$ profiles (variation of temperature against the transverse coordinate) again for two different values of viscosity parameter i.e. $\alpha = 0$

(plotted as solid lines) and $\alpha = 0.6$ (plotted as dotted lines). It is apparent that the temperature responds in a very different fashion to velocity i.e. it is *significantly enhanced* with an increase in viscosity parameter. As such the thermal boundary layer thickness in the nanofluid sheet will also be *increased*. In fig.3a, the effect of increasing Hartmann number is to substantially enhance temperatures. Greater magnetic field therefore heats the boundary layer regime. The supplementary work expended in dragging the nanofluid against the inhibiting action of the magnetic field is dissipated as thermal energy i.e. heat. This elevates thermal boundary layer thickness. This pattern has been computed by many other researchers for both nanofluid magnetohydrodynamics [**51**] and also classical viscous Newtonian magnetohydrodynamics [**52**]. Figs. 3b and fig 4a, demonstrate that with increasing thermal Grashof number (*Gr*) and species Grashof number (*Br*), temperature magnitudes are both decreased significantly. Greater thermal and species buoyancy forces therefore inhibit thermal diffusion in the boundary layer whereas they enhance momentum diffusion. Increasing both Grashof numbers decreases the thermal boundary layer thickness significantly. In fig4b, the effect of increasing thermophoresis parameter (*Nt*) is to elevate markdely the temperature values throughout the boundary layer transverse to the wall. Thermophoresis is associated with the global influence of averaged Brownian motion of particles under a steady temperature gradient. In hotter zones of the boundary layer, there are enhanced molecular impulses which cause a migration of nano-particles towards cooler zones where weaker molecular impulses are present. This energizes the nanofluid and results in an increase in temperatures, as elaborated by Giddings *et al.* [**53**]. Further corroboration of the trends computed in Fig. 4b is to be found in the work of Parola and Piazza [**54**]. Similar observations have also recently been made by Uddin *et al*. [**55**]. The thermophoretic effect is therefore considerable (*Nt* arises in both the energy conservation and species concentration equations (10) and 911)) and is in fact more pronounced at higher values of viscosity parameter (α). In all the plots shown in figs. 3 and 4 asymptotically smooth convergence of solutions is achieved in the free stream confirming that an adequately large infinity boundary condition has been used in the Runge-Kutta numerical code.

Figs 5a,b illustrate the response in the nano-particle concentration field, $\phi(\eta)$ to a variation in thermophoresis parameter (*Nt*) and Brownian motion parameter (*Nb*). Again solid lines denote the constant viscosity case ($\alpha = 0$) and dotted lines represent the variable viscosity case ($\alpha = 0.8$). At the wall and in close proximity to it, the concentration magnitudes are found to be strongly diminished in fig. 6a with an increase in thermophoresis parameter. A weak reduction is also computed with increasing viscosity parameter. However further from the wall, the reverse trend is computed. Peak concentration arises at intermediate distance form the wall (sheet). A substantial

elevation in nano-particle concentration is induced with greater thermophoresis effect and an increase in viscosity parameter also boosts concentrations. This pattern is susatined into the free stream. Fig. 5b reveals that increasing viscosity has a similar effect i.e. enhances nano-particle concentrations further from the wall into the free stream. However an increase in Brownian motion parameter, *Nb*, generates the opposite effect to thermophoresis parameter, *Nt* (in fig. 5a). Concentration magnitudes are enhanced at and near the wall whereas they are depressed further from the wall with increasing *Nb* values. Physically larger *Nb* values correspond to smaller nano-particle sies. This encourages thermal conduction and macro-convection as elaborated by Buonjiornio [**56**] and nano-particle species diffusion in the main body of the nanofluid i.e. further from the wall. The dominant influence of greater *Nt* values is therefore to enhance the nano-particle concentration boundary layer thickness whereas greater *Nb* values decrease nano-particle concentration boundary layer thickness.

Figs. 6a,b illustrate the influence of Prandtl number (*Pr*) and Schmidt number (*Sc*), respectively on the nano-particle concentration field, $\phi(\eta)$. Very little modification in profiles is observed near the wall in fig 6a with increasing Prandtl number; however a short distance transverse to the sheet the nano-particle concentration is initially elevated and thereafter strongly decreased with increasing Prandtl numbers. Increasing viscosity parameter also serves to enhance $\phi(\eta)$ values, but again the effect is prominent further from the sheet. Prandtl number embodies the relative role of momentum diffusion to thermal diffusion. For $Pr > 1$ (as studied in fig. 6a), momentum duffuses faster than heat. This via coupling of the momentum, energy and nano-particle species equations, indirectly influences the diffusion of nano-particles. In fig. 6a the Schmidt number is fixed at $Sc = 10$ implying that the momentum diffusivity is ten times that of the species diffusivity. Generally lower Prandtl number fluids attain greater nano-particle concentration boundary layer thicknesses. Similarly in fig. 6b an increase in Schmidt number is found to strongly depress $\phi(\eta)$ values. Maximum nano-particle concentration is therefore associated with the lowest value of Schmidt number ($Sc = 10$). Schmidt number is defined as the ratio of the *viscous (momentum) diffusion rate* to the *molecular (species) diffusion rate.* It also physically relates the relative thickness of the momentum (hydrodynamic) and concentration (nano-particle species) boundary layers. All cases in fig. 6b correspond to $Sc >> 1$ i.e. there is a much faster viscous diffusion rate compared with nano-particle mass diffusion rate. Greater Schmidt number substantially decreases concentration boundary layer thickness. Increasing viscosity parameter (α) on the other hand is found to once again elevate nano-particle concentration values, $\phi(\eta)$ and the effect is most pronounced again at *intermediate* distances from the wall.

Figs.7 (a & b) present the distributions for skin friction ($Re_x^{1/2}C_f$) versus viscosity parameter (α) for the effects of species Grashof number and thermal Grashof number at two different values of Hartmann (magnetohydrodynamic) number i.e. $M = 0$ (solid lines i.e. electrically non-conducting case) and $M = 0.5$ (dotted lines). It is noted in fig. 7a that the magnitude of skin friction is significantly elevated with increasing the magnetic field at all values of viscosity parameter. However skin friction is strongly *depressed* with *increasing* viscosity parameter. Conversely skin friction $Re_x^{1/2}C_f$) is markdely enhanced with an increase in species Grashof number (*Br*). In other words greater nano-particle species buoyancy force markedly accelerates the flow significantly. Fig. 7b also confirms that skin friction is strongly increased with greater Hartmann magnetic number (*M*) whereas it is substantially reduced with greater viscosity parameter (α). With an increase in thermal Grashof number (*Gr*), skin friction is also significantly elevated, confirming that greater thermal buoyancy force accelerates the boundary layer flow. Thermal buoyancy therefore aids considerably in momentum development.

Figs. 8a,b present the variation in Nusselt number ($Re_x^{-1/2}Nu_x$) against viscosity parameter with the effects of species Grashof number and thermal Grashof number. Computations are provided again for two different values of the Hartmann magnetic number i.e. $M = 0$ (solid lines) and $M = 0.5$ (dotted lines). Fig. 8a reveals that the magnitude of Nusselt number is considerably reduced with increasing the magnetic field strength i.e. higher values of Hartmann number, and similarly is elevated with increasing species Grashof number (*Br*). However Nusselt number is significantly depressed with greater viscosity parameter (α). Maximum Nusselt numbers therefore are achieved with the *constant viscosity nanofluid* case ($\alpha = 0$). Physically greater magnetic field, as computed earlier, enhances temperatures in the nanofluid. This results in a corresponding decrease in heat transfer to the wall away from the body of nanofluid i.e. lower Nusselt numbers. Increasing species (nano-particle) buoyancy force also cools the boundary layer and this manifests in an increase in the heat transferred to the wall i.e. greater Nusselt numbers. Inspection of Fig. 8b confirms that greater Hartmann number suppresses Nusselt number magnitudes as does increasing viscosity parameter. Increasing thermal Grashof number (*Gr*) however has a similar influence to increasing species Grashof number (*Br*). Greater *Gr* values enhance Nusselt numbers i.e. generate greater heat transfer to the wall. This implies greater cooling of the boundary layer, a trend observed in fig. 3b earlier.

Figs. 9a,b depict the Nusselt number profiles ($Re_x^{-1/2}Nu_x$) versus viscosity parameter with various thermophysical parameters. In fig. 9a the effects of thermophoresis parameter (*Nt*) are shown Nusselt number for two different values of Brownian motion parameter i.e. $Nb = 0.1$ (solid lines)

and $Nb = 0.5$ (dotted lines). Clearly the magnitude of Nusselt number *diminishes substantially* with increasing the magnitude of thermophoresis parameter and weakly decreases with greater Brownian motion parameter. Fig.9b presents the effect of Schmidt number on Nusselt number at two different values of Prandtl number i.e. *Pr = 3.97* (solid lines) and *Pr = 6.2* (dotted lines). It is observed that Nusselt number ($Re_x^{-1/2}Nu_x$) is significantly reduced with *increasing Schmidt number* whereas it is strongly *enhanced* with *Prandtl number*.

Figs.10 (a-c) illustrate streamline distributions in the x-η plane, with different values of viscosity parameter. We study the values $\alpha = 0$, $\alpha = 0.4$ and $\alpha = 0.8$, respectively. It is observed the the gaps between stream lines increase with increasing the magnitude of viscosity parameter.There is also a dis-intensification in the streamline plot at the upper right hand corner with greater viscosity. Viscosity therefore substantially modifies the fluid dynamics of the stretching sheet regime.

5. CONCLUSIONS

Magnetohydrodynamic transport of an electrically-conducting, variable-viscosity, water-based nanofluid over a stretching sheet has been investigated theoretically. The Reynolds exponential temperature-dependent viscosity model has been adopted. Both thermal and species (nano-particle) buoyancy forces have been incorporated and the Buonjiornio formulation employed which features significant thermophoretic and Brownian motion effects. A numerical solution to the transformed, dimensionless boundary layer equations under specific boundary conditions has been obtained, using the Runge–Kutta fourth order shooting method (RK). Validation with a Nakamura tridiagonal second-order accurate finite difference scheme (NFD) has been included. The computations have shown that:

1) Increasing viscosity parameter and Hartmann (magnetic) number reduces velocity whereas they increase momentum boundary layer thickness

2) Increasing both thermal and solutal Grashof numbers accelerates the flow and decreases momentum (hydrodynamic) boundary layer thickness.

3) Increasing viscosity parameter enhances temperature and nano-particle concentration and increases thermal and concentration boundary layer thickness in the nanofluid sheet.

4) Increasing Hartmann number enhance temperatures and reduces Nusselt numbers.

5) Increasing thermal and species Grashof number decreases temperatures and thermal boundary layer thicknesses and elevates Nusselt numbers magnitudes.

6) Increasing thermophoresis parameter enhances temperature, nano-particle concentration and thermal boundary layer thickness and nano-particle concentration boundary layer thickness whereas it decreases Nusselt number.

7) Increasing Brownian motion parameter decreases nano-particle concentration magnitudes and also concentration boundary layer thickness.

8) Increasing Prandtl number and Schmidt generally enhances nano-particle concentration.

9) Increasing thermophoresis parameter strongly reduces Nusselt number whereas increasing Brownian motion parameter weakly reduces Nusselt number.

The present study has neglected *rotational* (Centrifugal body force) effects [**57**]. These will be considered in the future.

REFERENCES

[1] S.U. Choi, Enhancing thermal conductivity of fluids with nanoparticles, *Development and Applications of Non-Newtonian Flow*, FED-Vol. 231/MD-Vol. 66, ASME, 99–105 (1995).

[2] M.A. Khairul, Shah K, Doroodchi E, Azizian R and Moghtaderi B., Effects of surfactant on stability and thermo-physical properties of metal oxide nanofluids *Int. J. Heat Mass Transf.*, 98, 778–87 (2016).

[3] S.K. Das, S.U.S. Choi, W. Yu, T. Pradeep, *Nanofluids – Science and Technology*, Wiley, New York (2008).

[4] E.E. Michaelides, *Nanofluidics – Thermodynamic and Transport Properties*, Springer, New York (2014).

[5] R.N. Mehta, Chakraborty, M. and Parikh, P. A. Nanofuels: Combustion, engine performance and emissions, *Fuel*, 120, 91 (2014).

[6] D. Tripathi and O. Anwar Bég, A study on peristaltic flow of nanofluids: Application in drug delivery systems, *Int. J. Heat Mass Transfer*, 70, 61-70 (2014).

[7] C. Kleinstreuer and Z. Xu, Thermal nanofluid flow in microchannels with applications, *Heat Transfer Enhancement with Nanofluids*, 237 (2015).

[8] R.S Vajjha, D.K. Das and D.R. Ray, Development of new correlations for the Nusselt number and the friction factor under turbulent flow of nanofluids in flat tubes, *Int. J. Heat Mass Transfer*, *80*, 353-367.

[9] O. Sadeghi, H.A. Mohammed, M. Bakhtiari-Nejad and M.A. Wahid, Heat transfer and nanofluid flow characteristics through a circular tube fitted with helical tape inserts, *Int. Comm. Heat Mass Transfer* 71, 234-244 (2016).

[10] D. Shin and D. Banerjee, Enhanced specific heat capacity of nanomaterials synthesized by dispersing silica nanoparticles in eutectic mixtures, *ASME J. Heat Transfer* 135(3), 032801 (Feb 08, 2013) (8 pages)

[11] G. Huminic and Huminic, Heat transfer and flow characteristics of conventional fluids and nanofluids in curved tubes: A review, *Renewable and Sustainable Energy Reviews*, *58*, 1327-1347 (2016).

[12] O. Mahian, Kleinstreuer, C., Kianifar, A., Sahin, A. Z., Lorenzini, G., & Wongwises, S. (2015). Entropy Generation Minimization in Nanofluid Flow, *Heat Transfer Enhancement with Nanofluids*, 411 (2015).

[13] P. Rana, R. Bhargava, O. Anwar Bég and A. Kadir, Finite element analysis of viscoelastic nanofluid flow with energy dissipation and internal heat source/sink effects, *Int. J. Applied Computational Mathematics*, 1-27 (2016). **DOI 10.1007/s40819-016-0184-5.**

[14] D. Tripathi, S. Bhushan, O. Anwar Bég and N. S. Akbar, Transient peristaltic diffusion of nanofluids: a model of micropumps in medical engineering, *J. Hydrodynamics, Ser. B* (2016) **Accepted**

[15] M. F. M. Basir, M.J. Uddin, A. I. Md. Ismail and O. Anwar Bég, Unsteady bio-nanofluid slip flow over a stretching cylinder with bioconvection Schmidt and Péclet number effects, *AIP Advances*, **6**, 055316-1 - 055316-15 (2016).

[16] Hamad M A A and Ferdows M., Similarity solution of boundary layer stagnation-point flow towards a heated porous stretching sheet saturated with a nanofluid with heat absorption / generation and suction / blowing : A lie group analysis *Commun. Nonlinear Sci. Numer. Simul.* **17** 132–40 (2012).

[17] N. S. Akbar, M. Shoaib, Dharmendra Tripathi, Shashi Bhushan and O. Anwar Bég, A study of entropy generation and heat transfer of CNT-nanofluids in flow driven by beating cilia through porous medium, *J. Hydrodynamics, Ser. B* (2016). **Accepted**

[18] I. Nkurikiyimfura, Y. Wang and Z. Pan, Heat transfer enhancement by magnetic nanofluids-A review, *Renewable and Sustainable Energy Reviews*, 21, 548–561 (2013).

[19] S. Noreen, Qasim, M., & Khan, Z. H., MHD pressure driven flow of nanofluid in curved channel, *J. Magnetism Magnetic Materials*, 393, 490-497 (2015).

[20] O. Anwar Bég, M. Ferdows, Shamima Islam and M. Nazrul Islam, Numerical simulation of Marangoni magnetohydrodynamic bio-nanofluid convection from a non-isothermal surface with magnetic induction effects: a bio-nanomaterial manufacturing transport model, *J. Mechanics Medicine Biology*, 14, 3, 1450039.1-1450039.32 (2014).

[21] N.S. Akbar, Raza, M. and Ellahi, R., Influence of induced magnetic field and heat flux with the suspension of carbon nanotubes for the peristaltic flow in a permeable channel, *J. Magnetism and Magnetic Materials*, 381, 405-415 (2015).

[22] S. A. Shehzad, T. Hayat and A. Alsaed, MHD flow of Jeffrey nanofluid with convective

boundary conditions, *J. Brazilian Soc. Mechanical Sciences and Engineering*, 37, 873-883 (2015).

[23] B.C. Sakiadis, Boundary-layer behavior on continuous solid surfaces: I. Boundary-layer equations for two-dimensional and axisymmetric flow, *AIChemE J.*, 7, 26–28 (1961).

[24] Gupta, E S., Gupta, A. S.: Heat and mass transfer on a stretching sheet with suction or blowing. *Can. J. Chem. Eng*. 55, 744-746 (1977).

[25] Wang, C. Y., The three dimensional flow due to a stretching flat surface, *Phys. Fluids*, 27, 1915-1917 (1984).

[26] Char, M.-I., Chen, C.-K.: Temperature field in non-Newtonian flow over a stretching plate with variable heat flux. *Int. J. Heat Mass Transfer*, 31, 917-921 (1988).

[27] Nadeem, S., Haq, R. U., Akbar, N. S., & Khan, Z. H. (2013). MHD three-dimensional Casson fluid flow past a porous linearly stretching sheet. *Alexandria Engineering J.*, *52*(4), 577-582 (2013).

[28] Cortell, R., MHD (magneto-hydrodynamic) flow and radiative nonlinear heat transfer of a viscoelastic fluid over a stretching sheet with heat generation/absorption. *Energy*, *74*, 896-905 (2014).

[29] Nadeem, S., Haq, R. U., & Khan, Z. H., Numerical study of MHD boundary layer flow of a Maxwell fluid past a stretching sheet in the presence of nanoparticles, *J. Taiwan Institute of Chemical Engineers*, *45*(1), 121-126 (2014).

[30] R. Bhargava, S. Sharma, H. S. Takhar, O. Anwar Bég and P. Bhargava, Numerical solutions for micropolar transport phenomena over a nonlinear stretching sheet, *Nonlinear Analysis: Modeling and Control J*., 12, 45-63 (2007).

[31] Khan, W. A., & Pop, I. (2010). Boundary-layer flow of a nanofluid past a stretching sheet. *Int. J. Heat and Mass Transfer*, *53*(11), 2477-2483.

[32] Makinde, O. D., & Aziz, A. (2011). Boundary layer flow of a nanofluid past a stretching sheet with a convective boundary condition. *Int. J. Thermal Sciences*, *50*(7), 1326-1332.

[33] O. Anwar Bég, M.S. Khan, I. Karim, M.M. Alam and M. Ferdows, Explicit numerical study of unsteady hydromagnetic mixed convective nanofluid flow from an exponentially stretching sheet in porous media, *Applied Nanoscience*, 4 (8) 943-957 (2014).

[34] Rana, P., & Bhargava, R., Flow and heat transfer of a nanofluid over a nonlinearly stretching sheet: a numerical study, *Comm. Nonlinear Science and Numerical Simulation*, 17(1), 212-226 (2012).

[35] Hamad, M. A. A., Analytical solution of natural convection flow of a nanofluid over a linearly stretching sheet in the presence of magnetic field, .*Int. Comm. Heat and Mass Transfer*, 38(4), 487-492 (2011).

[36] M.J. Uddin, O. Anwar Bég and N.S. Amin, Hydromagnetic transport phenomena from a stretching or shrinking nonlinear nanomaterial sheet with Navier slip and convective heating: a

model for bio-nano-materials processing, *J. Magnetism Magnetic Materials*, 368, 252-261(2014).

[37] Khan, W. A., Makinde, O. D., & Khan, Z. H., Non-aligned MHD stagnation point flow of variable viscosity nanofluids past a stretching sheet with radiative heat, *Int. J. Heat and Mass Transfer*, 96, 525-534 (2016).

[38] M.J. Uddin, O. Anwar Bég, N. Amran and A.I.MD. Ismail, Lie group analysis and numerical solutions for magneto-convective slip flow of a nanofluid over a moving plate with a Newtonian heating boundary condition, *Canadian J. Physics*, 93: 1–10 (2015).

[39] Mabood, F., Khan, W. A., & Ismail, A. I. M., MHD boundary layer flow and heat transfer of nanofluids over a nonlinear stretching sheet: a numerical study, *J. Magnetism and Magnetic Materials*, 374, 569-576 (2015).

[40] M.J. Uddin, P. Rana, O. Anwar Bég and A. I. Md. Ismail, Finite element simulation of magnetohydrodynamic convective nanofluid slip flow in porous media with nonlinear radiation, *Alex. Eng. J* (2016). (15 pages). http://dx.doi.org/10.1016/j.aej.2016.04.021

[41] Md. Jashim Uddin, O. Anwar Bég and Ahmad Izani Md. Ismail, Mathematical modelling of radiative hydromagnetic thermo-solutal nanofluid convection slip flow in saturated porous media, *Math. Prob. Engineering*, **2014**, Article ID 179172, 11 pages (2014).

[42] Gorla, R.S.R. and S. Nakamura, Combined convection from a rotating cone to micropolar fluids, *Math. Modelling Sci. Comput*., **2**, 1249–1254 (1993).

[43] Stachowiak G. W., Batchelor A. W., *Engineering Tribology*, University of Western Australia, Australia (2001).

[44] O. Anwar Bég and O.D. Makinde, Viscoelastic flow and species transfer in a Darcian high-permeability channel, *Petroleum Science and Engineering*, **76**, 93–99 (2011).

[45] Nakamura, S., Iterative finite difference schemes for similar and non-similar boundary layer equations, *Adv. Eng. Software*, **21**, 123–130 (1994).

[46] Bég, O. Anwar, NANONAK- A finite difference code for nanofluid convection problems of the boundary layer type, *Technical Report, NANO-C/5-1, 124pp, Gort Engovation, Bradford, England and Narvik, Norway, UK, August* (2013).

[47] Bég, O. Anwar, J. Zueco, M. Norouzi, M. Davoodi, A. A. Joneidi, Assma F. Elsayed, Network and Nakamura tridiagonal computational simulation of electrically-conducting biopolymer micro-morphic transport phenomena, *Computers in Biology and Medicine*, 44, 44–56 (2014).

[48] Nakamura, S., *Applied Numerical Methods and Software*, Prentice-Hall New Jersey, USA (1995).

[49] Bég, O. Anwar, Numerical methods for multi-physical magnetohydrodynamics, Chapter 1, pp. 1-112, *New Developments in Hydrodynamics Research, M. J. Ibragimov and M. A. Anisimov, Eds., Nova Science, New York, September* (2012).

[50] M.R. Krishnamurthy, B.C. Prasannakumara, B.J. Gireesha and R. S.R. Gorla, Effect of viscous dissipation on hydromagnetic fluid flow and heat transfer of nanofluid over an exponentially stretching sheet with fluid-particle suspension, *Cogent Mathematics*, 2, 1 (2015).

[51] K. Bhattacharyya and G. C. Layek, Magnetohydrodynamic boundary layer flow of nanofluid over an exponentially stretching permeable sheet, *Physics Research International*, Volume 2014 (2014), Article ID 592536, 12 pages. http://dx.doi.org/10.1155/2014/592536

[52] K.C. Cramer and S. Pai, *Magnetofluid Dynamics for Engineers and Applied Physicists*, MacGraw-Hill, New York (1973).

[53] J.C. Giddings, P.M. Shinudu, S.N. Semenov, Thermophoresis of metal particles in a liquid, *J. Colloid Interface Sci.*, 176, 454–458 (1995).

[54] A. Parola, R. Piazza, Particle thermophoresis in liquids, *Eur. Phys. J. E,* 15, 255–263 (2004).

[55] Md. Jashim Uddin, W.A. Khan, A.I.Md. Ismail, O. Anwar Bég, Computational study of three-dimensional stagnation point nanofluid bio-convection flow on a moving surface with anisotropic slip and thermal jump effects, *ASME J. Heat Transfer* (2016). DOI: 10.1115/1.4033581 (8 pages).

[56] J. Buongiorno Convective transport in nanofluids, *ASME J. Heat Transfer*, 128, 240–250 (2006).

[57] Puneet Rana, R. Bhargava and O. Anwar Beg, Finite element simulation of unsteady MHD transport phenomena on a stretching sheet in a rotating nanofluid, *Proc. IMECHE- Part N; J. Nanoengineering and Nanosystems*, 227, 77-99 (2013).